Donor and Acceptor Modes in Photonic Band Structure

E. Yablonovitch and T. J. Gmitter

Navesink Research Center, Bell Communications Research, Red Bank, New Jersey 07701-7040

R. D. Meade, A. M. Rappe, K. D. Brommer, and J. D. Joannopoulos

Department of Physics, Massachusetts Institute of Technology, Cambridge, Massachusetts 02139

Three-dimensionally periodic dielectric structures, photonic crystals, possessing a forbidden gap for electromagnetic wave propagation, a photonic band gap, are now known. If the perfect 3D periodicity is broken by a local defect, local electromagnetic modes can occur within the forbidden band gap. Addition of extra dielectric material locally, inside the photonic crystal, produces "donor" modes. Conversely, removal of dielectric material from the crystal produces "acceptor" modes. It is now possible to make high-Q electromagnetic cavities of ~ 1 cubic wavelength, for short wavelengths at which metallic cavities are useless. These new dielectric cavities can cover the range from mm waves to uv wavelengths.

There has been great progress recently in the creation of artificial three-dimensionally periodic dielectric structures which are to photon waves as semiconductor crystals are to electron waves. That is, these photonic crystals have a photonic band gap, a band of frequencies in which electromagnetic waves are forbidden [1], irrespective of propagation direction in space. Both face-centered-cubic lattice [2] and diamond symmetry [3] dielectric structures have now been shown to produce a photonic band gap.

The photonic band gap is very interesting in its own right. It is an energy band in which optical modes, spontaneous emission, and zero-point fluctuations are all absent. Nevertheless, the photonic band gap might actually be at its most interesting when the perfect translational symmetry is disrupted in a controlled manner. For example, by introducing a known degree of disorder, mobility edges and the Anderson localization transition [4] can be investigated.

Lasers, perhaps the most important application, also require that the 3D translational symmetry should be broken. Even while spontaneous emission into all 4π sr would be inhibited, a local electromagnetic mode is still necessary to accept the stimulated emission. In effect the local defect-induced structure resembles a Fabry-Pérot cavity, except that it reflects radiation back upon itself in all 4π spatial directions. Independently, Meade *et al.* [5] have proposed that this could be accomplished by introducing a simple defect into the system.

The perfect three-dimensional translational symmetry of a dielectric structure can be lifted in either one of two ways: (1) Extra dielectric material may be added to one of the unit cells. We find that such a defect behaves very much like a donor atom in a semiconductor. It gives rise to donor modes which have their origin at the bottom of the conduction band. (2) Conversely, translational symmetry can be broken by removing some dielectric material from one of the unit cells. Such defects resemble acceptor atoms in semiconductors. The associated acceptor

modes have their origin at the top of the valence band. We will find that acceptor modes are particularly well-suited to act as laser microresonator cavities. Indeed it appears that photonic crystals made of sapphire or other low-loss dielectrics will make the highest-Q single-mode cavities (of volume $\sim 1\lambda^3$) covering all electromagnetic frequencies above the useful working range of superconducting metallic cavities. The short-wavelength limit in the ultraviolet is set by the availability of optical materials with refractive index $\gtrsim 2$, the threshold index [2,3] for the existence of a photonic band gap.

For these experiments, we have chosen a face-centered-cubic (fcc) photonic crystal [2] employing nonspherical atoms. This fcc structure lends itself readily to microfabrication since it consists of intersecting drill holes [2] which can be made by reactive ion etching. While such microstructures have already been fabricated [6] in GaAs, we have chosen initially to investigate local defect modes in larger structures on the scale of 1 cm wavelengths. We selected a refractive index $n \approx 3.6$ for the microwave material, matching that of the common semiconductors Si and GaAs. Experiment is supplemented by theoretical calculations of the photonic bound states.

Photonic crystals generally consist of a continuous three-dimensional web of dielectric material, made up of interconnecting ribs. The Wigner-Seitz unit cell of our photonic crystal [2] is the standard fcc rhombic dodecahedron [2] with "air atoms" created by drill holes centered on the top three faces, which exit through the bottom three faces. Figure 1 is a $\langle 1\bar{1}0 \rangle$ cross section of our photonic crystal cutting through the center of a unit cube. Shading represents dielectric material. The large dots are centered on the air atoms and the rectangular dashed line is a face-diagonal cross section of the unit cube. Such structures are made simply by drilling three sets of holes 35.26° off vertical into the $\langle 111 \rangle$ top face.

Since we could design the structure at will, donor defects were chosen to consist of a single dielectric sphere
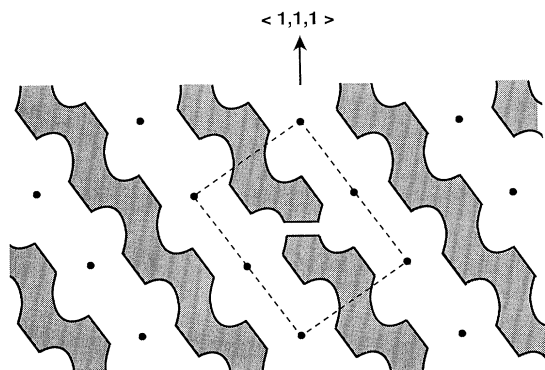
FIG. 1. A $\langle 1\bar{1}0 \rangle$ cross-sectional view of our face-centered-cubic photonic crystal [2] consisting of nonspherical "air atoms" centered on the large dots. Dielectric material is represented by the shaded area. The rectangular dashed line is a face-diagonal cross section of the unit cube. Donor defects consisted of a dielectric sphere centered in an atom. We selected an acceptor defect as shown, centered in the unit cube. It consists of a missing horizontal slice in a single vertical rib.
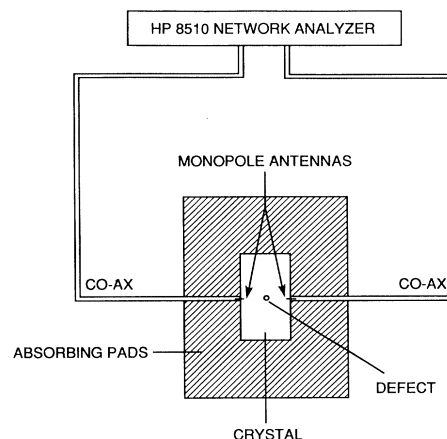

FIG. 2. Experimental configuration for the detection of local electromagnetic modes in the vicinity of a lattice defect. Transmission amplitude attenuation from one antenna to the other is measured. At the local mode frequency the signal hops by means of the local mode in the center of the photonic crystal producing a local transmission peak. The signal propagates in the $\langle 111 \rangle$ direction through 8–10 atomic layers.

centered in an air atom. Likewise, by breaking one of the interconnecting ribs, it is easy to create acceptor modes. We selected an acceptor defect as shown in Fig. 1, centered in the unit cube. It comprises a vertical rib which has a missing horizontal slice.

The heart of our experimental apparatus is a photonic crystal embedded in microwave absorbing pads as shown in Fig. 2. The photonic crystals were 8–10 atomic layers thick in the $\langle 111 \rangle$ direction. The cubic unit-cell length was $a = 11$ mm and the hole diameter was 5.16 mm, leaving an empty volume fraction ~78%. Monopole antennas, consisting of 6-mm pins, coupled radiation to the defect mode. The HP 8510 Network Analyzer was set up to measure transmission between the antennas. Figure 3(a) shows the transmission amplitude in the absence of a defect. There is very strong attenuation ($\sim 10^{-5}$) between 13 and 16 GHz marking the valence- and conduction-band edges of the forbidden gap. This is a tribute to both the dynamic range of the network analyzer, and the sizable imaginary wave vector in the forbidden gap.

A transmission spectrum in the presence of an acceptor defect is shown in Fig. 3(b). Most of the spectrum is unaffected, except at the electromagnetic frequency marked "deep acceptor" within the forbidden gap. At that precise frequency, radiation "hops" from the transmitting antenna to the acceptor mode and then to the receiving antenna. The acceptor level frequency, within the forbidden gap, is dependent on the volume of material removed. Figure 4 shows the acceptor level frequency as a function of defect volume removed from one unit cell. When a relatively large volume of material is removed, the acceptor level is deep, as shown in Fig. 3(b). A smaller amount of material removed results in a shal-

low acceptor level, nearer the valence band. If the removed material volume falls below a threshold volume, the acceptor level falls within the continuum of levels below the top of the valence band, becoming metastable.

On an expanded frequency scale we can measure the resonator Q of the deep acceptor mode, which is $Q \sim 1000$, as limited by the loss tangent of the Emerson & Cumming Stycast material of which the photonic crystal was made.

The behavior of an off-center donor defect is shown in Fig. 3(c). In that case the donor volume was slightly above the required threshold for forming bound donor modes. Already two shallow donor modes can be seen in Fig. 3(c). When the donor is centered in the Wigner-Seitz unit cell, the two modes merge to form doubly degenerate donor modes as in Fig. 4. Single donor defects seem to produce multiple donor levels. Figure 4 gives the donor level frequency as a function of donor volume. As in the case of acceptors, there is threshold defect volume required for the creation of bound modes below the conduction-band edge. However, the threshold volume for donor defects is almost 10 times larger than the acceptor threshold volume. Apparently this is due to the electric-field concentration in the dielectric ribs at the top of the valence band. Bloch wave functions at the top of the valence band are rather easily disrupted by the missing rib segment.

We have chosen in Fig. 4 to normalize the defect volume to a natural volume of the physical system, $(\lambda/2n)^3$, which is basically a cubic half wavelength in the dielectric medium. More specifically, λ is the vacuum wavelength at the midgap frequency, and n is the refrac-
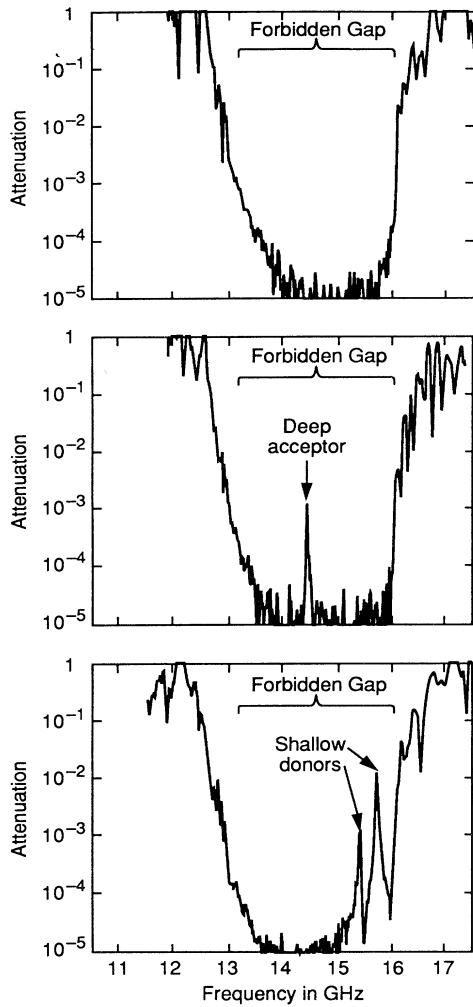
(a)

(b)

(c)

FIG. 3. (a) Transmission attenuation through a defect-free photonic crystal, as a function of microwave frequency. The forbidden gap falls between 13 and 16 GHz. (b) Attenuation through a photonic crystal with a single acceptor in the center. The large acceptor volume moved its frequency near midgap. The electromagnetic resonator Q was ~1000, limited only by the loss tangent of the dielectric material. (c) Attenuation through a photonic crystal with a single donor defect, an uncentered dielectric sphere, leading to two shallow donor modes.
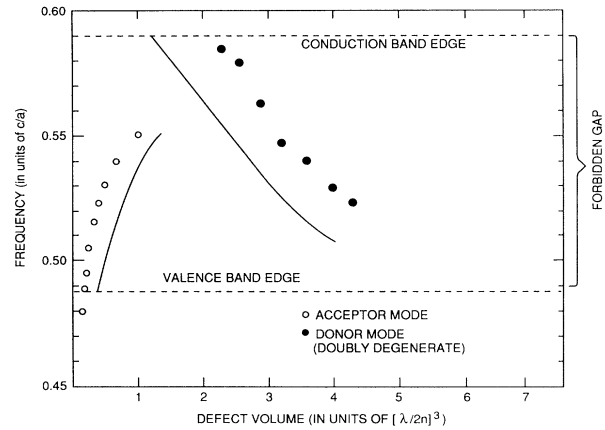

FIG. 4. Donor and acceptor mode frequencies as a function of normalized donor and acceptor defect volume. The points are experimental and the corresponding lines are calculated. Defect volume is normalized to $(\lambda/2n)^3$, where λ is the midgap vacuum wavelength and n is the refractive index. A finite defect volume is required to bind a mode in the forbidden gap.

tive index of the dielectric medium. Since we are measuring a dielectric volume, it makes sense to normalize to a half-wavelength cube as measured at the dielectric refractive index. Based on the reasonable scaling of Fig. 4, our choice of volume normalization would seem justified. (Experimentally, the odd-shaped defect volumes were measured by weighing the samples.)

It is interesting to compare our local modes to those of a one-dimensional Fabry-Pérot resonator, constructed in the usual manner of quarter-wave multilayer dielectric mirrors. In such a resonator the mirrors face each other and are usually separated by an integral number of half

wavelengths. The net effect of the left and right mirrors facing each other is that they combine to form a monolithic 1D periodic dielectric structure, but with a quarter wavelength of phase slip introduced into the very center. This same quarter wavelength of phase slip is often employed in distributed feedback lasers [7], effectively converting them into Fabry-Pérot resonators. The standing-wave mode is sometimes [8] regarded as a bound state split off into the 1D band gap and localized to the quarter-wave defect in the periodic structure. In one dimension, however, nothing requires that the defect be one-quarter wavelength long. A phase slip, no matter how small, allows a bound mode to form in the forbidden gap, usually near a band edge. This is in distinction to Fig. 4 where a finite-sized defect volume is required to bind a mode.

This is similar to the comparison between 1D and 3D quantum mechanics. In one dimension even an infinitesimal quantum well will bind [9] a state. In three dimensions, a finite-depth potential well is required to produce [9] a bound state. Figure 4 is telling us that the same requirement for a finite defect volume applies to 3D confined photon modes. John and Wang [10] have shown that the requirement for a finite-volume-integrated polarizability can be satisfied even by a single resonant atom if undamped by nonradiative decay. Then an individual atom is capable of binding a local electromagnetic mode at its resonant transition frequency. They call this a photon-atom bound state. Inhibited spontaneous emission is accompanied with strong self-dressing of the atom by its own localized radiation fields, leading to anomalous Lamb shifts.

We have also performed calculations of the frequency spectrum of these dielectric systems. In order to solve for

the electromagnetic modes, we expand Maxwell's equations in plane waves, employing the techniques of Ho, Chan, and Soukoulis [3]. We employ the supercell method, placing one defect in a repeated cell of dielectric material. Our calculations were performed in supercells containing eight fcc Wigner-Seitz cells, and we have performed tests on larger supercells containing eight conventional fcc cubic unit cells (32 Wigner-Seitz cells). Because the distance between defects is relatively small, there is significant overlap between the localized modes on neighboring defects. This overlap manifests itself as a dispersion of the impurity band, and the frequency of the bound state is taken to be the band center. We expanded the $H(r)$ magnetic field in a basis of 4000 plane waves, and the lowest eigenvalues were obtained by the Natarajan and Vanderbilt [11] iterative diagonalization technique.

The solid lines in Fig. 4 show good qualitative agreement with the experimental points. The discrepancy between theory and experiment is larger for defects in supercells than for purely bulk systems, where better than 1% agreement has been achieved. There are two important reasons for this larger discrepancy. First, because of the larger unit-cell size, it is necessary to work at a lower plane-wave cutoff. Second is the small number of primitive unit cells used in the supercell approximations. As in Ref. [5], the dispersion of the impurity band is quite large in the eight-atom supercell, $\sim(20$–$80)\%$ of the gap width for various states. Increasing the supercell to 32 atoms reduces the bandwidth by 80%.

The extension of these 3D dielectric resonators to laser wavelengths is marked by the following considerations. The refractive index we have chosen to work with ($n=3.6$) is a good match to the common semiconductors of which lasers are made. Furthermore, the fcc geometry we are using has begun [6] to be microfabricated in GaAs. Such microresonators will be particularly valuable for making tiny low-threshold lasers. But their value is greatly increased if the photonic band gap inhibits spontaneous emission. In a semiconductor laser, this would lead to near unity quantum efficiency into the lasing mode. Photon number state squeezing [12] into that mode would be greatly enhanced. Inhibited spontaneous emission requires that the broad semiconductor luminescence band should be centered within the forbidden gap. In semiconductor lasers, population inversion and gain first appear at the red edge of the luminescence band, i.e.,

nearer to the valence band. This suggests that acceptor modes would be the appropriate type for lasers.

The other advantage for acceptor-mode laser cavities is associated with our acceptor defect geometry. The vertical rib with a missing horizontal slice, as in Fig. 1, can be readily microfabricated. It should be possible to create it in III-V materials by growing an aluminum-rich epitaxial layer and lithographically patterning it down to a single dot the size of one of the vertical ribs. After regrowth of the original III-V composition and reactive ion etching of the photonic crystal, HF acid etching, whose [13] selectivity $\geq 10^8$, will be used to remove the Al-rich horizontal slice from the one rib containing such a layer. The resonant frequency of the microcavity can be controlled by the thickness of the Al-rich sacrificial layer.

[1] E. Yablonovitch, Phys. Rev. Lett. **58**, 2059 (1987).

[2] E. Yablonovitch, T. J. Gmitter, and K. M. Leung, Phys. Rev. Lett. **67**, 2295 (1991).

[3] K. M. Ho, C. T. Chan, and C. M. Soukoulis, Phys. Rev. Lett. **65**, 3152 (1990).

[4] S. John, Phys. Rev. Lett. **58**, 2486 (1987).

[5] R. D. Meade, K. D. Brommer, A. M. Rappe, and J. D. Joannopoulos, Phys. Rev. B (to be published).

[6] A. Scherer and B. P. van der Gaag (private communication).

[7] H. Kogelnik and C. V. Shank, J. Appl. Phys. **43**, 2328 (1972).

[8] H. A. Haus and C. V. Shank, IEEE J. Quantum Electron. **12**, 532 (1976); S. L. McCall and P. M. Platzmann, IEEE J. Quantum Electron. **21**, 1899 (1985).

[9] L. I. Schiff, *Quantum Mechanics* (McGraw-Hill, New York, 1949), see pp. 37 and 77.

[10] S. John and J. Wang, Phys. Rev. Lett. **64**, 2418 (1990).

[11] R. Natarajan and D. Vanderbilt, J. Comput. Phys. **81**, 218 (1989).

[12] Y. Yamamoto and S. Machida, Phys. Rev. A **35**, 5114 (1987).

[13] E. Yablonovitch, T. Gmitter, J. P. Harbison, and R. Bhat, Appl. Phys. Lett. **51**, 2222 (1987).